KAPL-P-000053
(K96070)
CONF-970670--

PIV VELOCITY MEASUREMENTS IN THE WAKE OF AN OBSTRUCTION SIMULATING A TAYLOR BUBBLE IN A DUCT

P. Vassallo, R. Kumar

June, 1997

NOTICE

KAPL ATOMIC POWER LABORATORY SCHENECTADY, NEW YORK 12301

Operated for the U. S. Department of Energy
by KAPL, Inc. a Lockheed Martin company

DISCLAIMER

DISCLAIMER

Portions of this document may be illegible in electronic image products. Images are produced from the best available original document.

PIV Velocity Measurements in the Wake of an Obstruction Simulating a Taylor Bubble in a Duct

by

Peter Vassallo and Ranganathan Kumar

Abstract

Knowledge of the flow structure behind a gas slug rising in a liquid is useful in two-phase flow modelling, especially with respect to bubble wake dynamics. In churn-turbulent flow, where the gas phase is composed of larger slugs interspersed with smaller bubbles, the larger bubbles or slugs are observed to entrain the smaller bubbles in their wake. The smaller bubbles are accelerated toward the trailing end of the larger bubbles or slugs where they subsequently coalesce. To help characterize these interactions, PIV measurements in the wake of a large stationary slug obstruction have been obtained in a duct. Two flow rates were established: one represented the flow behind a large gas slug rising in quiescent fluid and the other represented an idealized slug rising with a higher relative velocity, as typically found in higher void fraction churn-turbulent flow.

The PIV video camera and light sheet were moved axially to capture images from the rear of the slug obstruction to approximately 25.4 cm downstream. The image magnification was about 6.5, which corresponded to a 5.84 cm x 4.88 cm image size for a 0.9 cm x 0.75 cm camera pixel array. The measurements were taken in the center of the test section to within ±0.25 mm. Twenty images were taken at each axial location and averaged to obtain the local mean velocities. Because the test section was thin (aspect ratio < 0.05), little variation is expected in the wake velocity measurements over the thickness uncertainty range. Figure 1 shows the layout of the PIV set-up, including details on the light sheet optics and camera orientation.

Full scale vector plots, normalized by the mean velocity, of the measured velocity field in the wake of the slug for the two specified Reynolds numbers are given in Figures 2 and 3. The wake extent is similar for both cases, although stronger recirculation is evident for the higher Reynolds number case. Indeed, for this case, the peak reverse velocity is about twice as fast as the slug velocity; a bubble captured here would quickly move to coalesce with the slug. Note that the largest reverse velocity in the wake is well downstream of the rear of the slug, indicating that the fluid is spreading as it moves upstream in the wake and is continually merging with the high velocity jet flow on either side of the slug. Villermaux and Hopfinger (1994) identified similar behavior in their study of two co-flowing jets, where a turbulent packet of fluid, shed at the merging distance of the jets, was convected upstream toward the beginning of the shear instability at the edge of the jets.

The behavior of the flow around the slug is largely representative of wall bounded jet flow. The spreading rate for these flows is usually determined by examining the growth of the half-width of the wall jet (where the velocity is half the maximum velocity) in stagnant surroundings. A similar

analysis was performed for the two cases in Figures 2 and 3; the results are plotted in Figure 4. Three regions are indicated by the data: an entrance region which is affected by the inlet conditions; a region where the jet grows at a linear rate bounded by the values reported by Launder and Rodi (1981) for 2-D and 3-D wall jets, and a region where the jets have merged. With respect to region 1, Sforza and Herbst (1970) have observed that the flow development near the jet exit depends on the details of the jet exit geometry. In our case, the entrance affects are further complicated by the fact that the flow is converging just upstream of the jet exit (due to the curvature of the slug). In region 2, which is about 20 diameters downstream of the jet exit, similar velocity profiles are established from the wall to the shear layer. The growth rate is about 0.06 for both Reynolds numbers studied, indicating some 3-D affects due to the small jet entrance thickness dimension (i.e., in most 2-D studies, the thickness dimension is large compared to the jet entrance height). The relative insensitivity of the growth rate to Reynolds number agrees with Launder and Rodi's observation, although the Reynolds numbers in their review were somewhat higher than the present experiments'. In region 3, there is considerable scatter due to the turbulent interactions between the jets. The rapid change of flow conditions in this region disrupts equilibrium, such that the turbulent processes and the mean flow take a long time to respond. This invalidates the self-preservation assumption for wall jets and the spreading rate does not follow the asymptotic values from similarity. However, it is interesting to note that the slope in Figure 4 is larger than in the other regions, and is consistent with the increase in growth rate observed in far wake flows (Wilcox, 1993).

PIV Velocity Measurements in the Wake of an Obstruction Simulating a Taylor Bubble in a Duct

by

Peter Vassallo and Ranganathan Kumar

Summary

Mean velocity measurements in the wake of an obstruction simulating a Taylor bubble (or slug) have been obtained using Particle Image Velocimetry (PIV) in a duct. Two flow rates were established: one represented the flow behind a large gas slug rising in quiescent fluid and the other represented an idealized slug rising with a higher relative velocity, as typically found in higher void fraction churn-turbulent flow. The results indicate that, in a reference frame fixed to the slug, the flow around the sides of the slug behaves like wall bounded jets which eventually merge downstream of the slug. The ratio of wake volume to slug volume is nearly the same for both Reynolds numbers tested (i.e., 3.0 at Re=3,628 and 2.9 at Re=7,257) although the measurements suggest that the wake size decreases somewhat as the Reynolds number is increased.

Nomenclature

$\Delta\rho$	density difference between gas and liquid
ρ_l	liquid density
W	test section width
g	gravitational constant
V_∞	infinite rise velocity
V_r	rise velocity
α	gas void fraction
σ	uncertainty in measurement
Δt	time between laser pulses
M	magnification factor
U	mean velocity
u'	rms velocity
N	number of samples used to calculate velocity
ϑ	fluid kinematic viscosity
X	distance downstream of the jet
$y_{1/2}$	distance from wall in which the jet velocity is one-half its maximum at a given X location

1.0 Introduction

Knowledge of the flow structure behind a gas slug rising in a liquid is useful in two-phase flow modelling, especially with respect to bubble wake dynamics. In churn-turbulent flow, where the gas phase is composed of larger slugs interspersed with smaller bubbles, the larger bubbles or slugs are observed to entrain the smaller bubbles in their wake. The smaller bubbles are accelerated toward the trailing end of the larger bubbles or slugs where they subsequently coalesce. To help characterize these interactions, PIV measurements in the wake of a large stationary slug obstruction have been obtained in a duct. The extent of the wake, the velocity in the wake and recirculation strength are determined for two separate Reynolds numbers.

2.0 Experimental Method

2.1 Test Set-Up

The slug obstruction was friction fitted at the entrance to the test section, as shown in Figure 1. Using a stationary slug simplified the measurements and allowed for multiple PIV image acquisition at a given location behind the slug. This is not literally the same as a slug moving in a liquid, but it is a reasonable approximation. In order to relate these wake measurements with the approximate wake behind a moving slug, the slug velocity must be added to the measured velocity field.

The dimensions of the slug obstruction are shown in Figure 1. These dimensions were selected based on previous isolated bubble rise experiments, as well as air-water experiments in churn-turbulent flow. Because the slug obstruction was friction fitted into the test section, no flow occurred along the sides.

The water flow rates over the obstruction were selected to cover a wide range of relative velocity. For a slug rising in an infinite fluid, Maneri (1995) has expressed the relative velocity as:

$$V_\infty = 0.2445\left[1 + 0.82\,(t/W) - 0.368\,(t/W)^2\right]\left[gW\frac{\Delta\rho}{\rho_l}\right]^{1/2} \qquad (1)$$

For the current test section dimensions and room temperature air-water properties, the above equation yields $V_\infty = 0.2$ m/s. A flow rate equivalent to this velocity was established in the test section to simulate the infinite rise condition. A second, higher flow rate was established to simulate the relative velocity of an idealized slug in a higher void fraction churn turbulent flow. Drift flux theory (Vassallo and Kumar, 1995) provides some indication of the magnitude of the relative velocity as:

$$V_r = \frac{V_\infty}{(1-\alpha)} \qquad (2)$$

Using $\alpha = 0.5$, which is a reasonably high void fraction in churn turbulent flow, $V_r = 0.4$ m/s.

2.2 PIV Technique

The PIV system was composed of a Nd:Yag pulsed laser, 1.4 MB video camera, rotating mirror shifter, and an IBM Risc6000 workstation. In taking the measurements, a region of the flow was illuminated with two 6 nsec pulses of laser light, and the video camera, focused on the light sheet, recorded the position of the light scattering particles at two separate times. The rotating mirror was used to produce a shift between the first and second particle images so that the velocity direction could be determined. Because the video images contained a high density of image pairs, a correlation algorithm was used to determine the local flow velocity. The video image was divided into interrogation spots, or small regions of the flow over which spatially averaged particle displacements were computed. The particle image intensities were digitized, and 1-frame cross correlation was employed to obtain the velocity in each interrogation spot. A good review of the PIV technique is given by Adrian (1991).

2.2.1 Description of Correlation Algorithm

In standard cross correlation algorithms, two image frames are used to calculate velocity with 1 pulse of light on each frame. The distance the particles travel between frames multiplied by the framing rate determines the flow velocity. Because the particle images are separated between frames, the velocity is measured without directional ambiguity, and image shifting is not required. Another advantage is that the signal-to-noise ratio for 2-frame cross correlation is superior to the auto-correlation methods. This is because only the first particle images are in frame 1 and only the second particle images are in frame 2. Thus, there is not a mixture of particle images as there are with the usual single frame correlation methods.

However, in general, 2-frame cross correlation is limited by the effective image framing rate. With the present CCD camera, the time between frames is 0.33 sec, or 3 Hz. From the standpoint of image processing, the particle must move less than 1/4 of the interrogation region between the first and second laser pulses. This implies that the velocity should be less than 20 cm/s for a 1.25 mm projected pixel size. This is really only practical for bubble rise experiments where the velocity is low and the bubble size is comparable to the pixel size. In general, 2-frame cross correlation is not suitable for higher velocity single phase flows.

Recently, an algorithm has been developed (Lourenco, 1996) which overcomes the framing rate limitation but still offers the computational advantages of cross correlation; 1-frame cross correlation. With this method, a large image shift is imposed between light pulses, which creates a particle pair separation distance greater than the interrogation spot size. Three Fourier transforms are then used to determine the average particle displacement: one for the interrogation region, another for the region separated by the image shift, and an inverse transform from the complex conjugate product of the two. This, in effect, correlates a group of particles from one interrogation region with a similar grouping in the other. It is akin to moving the second interrogation region over the first until the best "match" is found. This reveals one advantage of 1-frame cross correlation: when the interrogation regions are separated, the displacement of very large particles

with varying pixel intensity (such as gas bubble in liquid) are more accurately determined. This is because the algorithm is not confused by the intensity variations within the large particles or bubbles and treats them like a group. Also, with 1-frame cross-correlation the velocity of large particles or bubbles with displacements much smaller than the particle diameter can be resolved. The 1-frame cross correlation algorithm was used for both of the cases tested in this study.

2.3 Data Acquisition and Uncertainty

The PIV video camera and light sheet were moved axially to capture images from the rear of the slug obstruction to approximately 25.4 cm downstream. The image magnification was about 6.5, which corresponded to a 5.84 cm x 4.88 cm image size for a 0.9 cm x 0.75 cm camera pixel array. The measurements were taken in the center of the test section to within ±0.25 mm. Twenty images were taken at each axial location and averaged to obtain the local mean velocities. Because the test section was thin (aspect ratio > 20), little variation is expected in the wake velocity measurements over the thickness uncertainty range. Figure 1 shows the layout of the PIV set-up, including details on the light sheet optics and camera orientation.

Because the rotating mirror was used to produce large image shifts (> 60 pixels), a non-uniform shift displacement was observed across the image field (as reported by Raffel and Kompenhans (1995)). In order to correct for this non-uniformity, 11 images were acquired in zero velocity liquid flow, averaged, and then subtracted from the average displacement field measured in the flowing condition.

The uncertainty in measured displacement for a 95% confidence level may be given as:

$$\left(\frac{\sigma_U}{\overline{U}}\right)^2 = \left(\frac{Cd_{img}}{\Delta t \overline{U}}\right)^2 + \left(\frac{\sigma_{mag}}{M}\right)^2 + \left(\frac{\sigma_{shift}}{\Delta t \overline{U}}\right)^2 + \left(\frac{2u'}{\sqrt{N}\overline{U}}\right)^2 \qquad (3)$$

Term 1 on the right hand side is the uncertainty in determining the center of the particle image. The constant, C, accounts for algorithm uncertainties, and is estimated to be 0.07 (TSI, 1994). The image diameter is a function of seed diameter and optical parameters. For the 1 μm titanium dioxide seed particles used in these tests, the image diameter is 55 μm (or 1.19 pixels), and the uncertainty is ±6% .

Term 2 is the uncertainty in determining the optical magnification factor. This uncertainty is small, estimated to be ±1%.

Term 3 is the uncertainty associated with irregularities in the image shift due to non-uniform mirror rotation. Based on the distribution of the calculated mean displacements from the zero velocity images, the uncertainty is estimated to be ±7.3% .

Term 4 is the statistical uncertainty in determining the average particle displacement. A turbulence intensity of 50% was assumed, which is conservative from the standpoint of free jet measurements; based on 20 images and 20 samples in each interrogation spot, the uncertainty is ±5% .

The total uncertainty in mean velocity is therefore estimated to be ±10.7%.

3.0 Results

Full scale vector plots, normalized by the mean velocity, of the measured velocity field in the wake of the slug for the two specified Reynolds numbers[1] are given in Figures 2 and 3. Some asymmetry is present in the flow field due to small asymmetries in the slug obstruction and slight misalignment in the position of the slug (which was centered in the test section to within 0.1mm, as shown in Figure 1). The wake extent in Figures 2 and 3 is similar for both cases, although stronger recirculation is evident for the higher Reynolds number case. Indeed, for this case, the peak reverse velocity is about twice as fast as the slug velocity (given by Eq. (2)); a bubble captured here would quickly move to coalesce with the slug. Note that the largest reverse velocity in the wake is well downstream of the rear of the slug, indicating that the fluid is spreading as it moves upstream in the wake and is continually merging with the high velocity jet flow on either side of the slug. Villermaux and Hopfinger (1994) identified similar behavior in their study of two co-flowing jets, where a turbulent packet of fluid, shed at the merging distance of the jets, was convected upstream toward the beginning of the shear instability at the edge of the jets.

3.1 Wall Jet Analysis

The behavior of the flow around the slug is largely representative of wall bounded jet flow. Each wall jet contains an inner region in which the flow behaves like a conventional turbulent boundary layer, and an outer region in which the free shear layer is closer to a free shear flow than a wall bounded flow. The spreading rate is usually determined by examining the growth of the half-width of the wall jet (where the velocity is half the maximum velocity) in stagnant surroundings. When two jets are allowed to merge from either side of the slug, there is a recirculation region formed behind the slug, and the velocity patterns and spreading process become complex. These characteristics of the flow behind a slug in a duct have not been studied previously and are useful for two-phase flow model development.

Launder and Rodi (1981) have reviewed the measured growth rates of the outer layer in 2-D and 3-D wall jets for various geometries, and have reported growth rates of

$$\frac{dy_{1/2}}{dX} = 0.073 \pm 0.002 \quad \text{for 2-D jets} \tag{4}$$

$$\frac{dy_{1/2}}{dX} = 0.048 \pm 0.002 \quad \text{for 3-D jets}$$

A similar analysis was performed for the two cases in Figures 2 and 3; the results are plotted in Figure 4. Three regions are indicated by the data: an entrance region which is affected by the inlet conditions; a region where the jet grows at a linear rate bounded by the values reported by Laun-

[1] Reynolds number is defined as $Re = \frac{V_j D_j}{\vartheta}$, where V_j = mean jet exit velocity, D_j = hydraulic jet diameter

der and Rodi (1981) for 2-D and 3-D wall jets, as in Eq. (4), and a region where the jets have merged. With respect to region 1, Sforza and Herbst (1970) have observed that the flow development near the jet exit depends on the details of the jet exit geometry. In our case, the entrance effects are further complicated by the fact that the flow is converging just upstream of the jet exit (due to the curvature of the slug). In region 2, which is about 20 diameters downstream of the jet exit, similar velocity profiles are established from the wall to the shear layer. The growth rate is about 0.06 for both Reynolds numbers studied, indicating some 3-D effects due to the small jet entrance thickness dimension (i.e., in most 2-D studies, the thickness dimension is large compared to the jet entrance height). The relative insensitivity of the growth rate to Reynolds number agrees with Launder and Rodi's observation, although the Reynolds numbers in their review were somewhat higher than the present experiments'. In region 3, there is considerable scatter due to the turbulent interactions between the jets. The rapid change of flow conditions in this region disrupts equilibrium, such that the turbulent processes and the mean flow take a long time to respond. This invalidates the self-preservation assumption for wall jets and the spreading rate does not follow the asymptotic values from similarity. However, it is interesting to note that the slope in region 3 of Figure 4 is larger than in the other regions, and is consistent with the increase in growth rate observed in far wake flows (Wilcox, 1993).

3.2 Wake Extent

Two parameters which are used to describe wake extent are the dimensionless wake volume (W_V) and the dimensional wake length (W_L). The former may be calculated for the cases in Figures 2 and 3 by measuring the area of the wake (where the velocity is < 0) and dividing by the area of the slug (which is 24.2 cm^2). This gives the dimensionless wake volume for the slug in a reference frame fixed to the slug. To obtain the dimensionless wake volume in a laboratory reference frame, the mean slug velocity must first be added to the measured velocity field. The wake length is calculated by measuring the distance to the merging region from the base of the slug and dividing by the area equivalent slug diameter (which is 5.56 cm). The results are shown in Table 1.

Table 1: Dimensionless Wake Parameters

Reference Frame	Jet Reynolds Number	W_V	W_L
Slug	3628	3.0	3.8
Slug	7257	2.9	3.6
Laboratory	3628	4.9 - 6.4	5.5 - 7.2
Laboratory	7257	3.7 - 6.2	5.5 - 7.1

Ranges are given in the laboratory reference frame because the wake parameters had to be estimated by extrapolating the velocity data far downstream of the slug. The wake length and volume for both Reynolds numbers are very similar, although it does appear that the wake size

decreases somewhat as the Reynolds number is increased.

Acknowledgement: The authors are grateful to Dr. Luiz Lourenco for his efforts in developing the processing algorithms.

References

Adrian, R.J., 1991, "Particle-Imaging Techniques for Experimental Fluid Mechanics," Ann. Rev. Fluid Mech., Vol. 23, pp 261-304.

Launder, B.E., amd Rodi, W., 1981, "The Turbulent Wall Jet," Prog. Aero. Sci., Vol. 19, pp 81-128.

Lourenco, L., Private Communications.

Maneri, C.C., 1995, "New Look at Wave Analogy for Prediction of Bubble Terminal Velocities", AIChE Journal, Vol. 41, No. 3.

Raffel, M., and Kompenhans, J., 1995, "Theoretical and Experimental Aspects of Image-Shifting by Means of a Rotating Mirror System for Particle Image Velocimetry," Meas. Sci. Tech., Vol. 6, pp 795-808.

Sforza, M.P., and Herbst, G., 1970, "A Study of Three-Dimensional, Incompressible, Turbulent Wall Jets," AIAA J., Vol. 8, pg 276.

TSI PIV Seminar Notes, 1994.

Vassallo, P.F., and Kumar, R., 1995, "Liquid and Gas Velocity Measurements Using LDV in Air-Water Duct Flow", FED-Vol. 233, 1995 IMECE.

Villermux, E., and Hopfinger, E.J., 1994, "Periodically Arranged Co-Flowing Jets", J. Fluid Mech., Vol 263, pp. 63-92.

Wilcox, D.C., 1993, "Turbulence Modeling for CFD", Griffin Printing, CA.

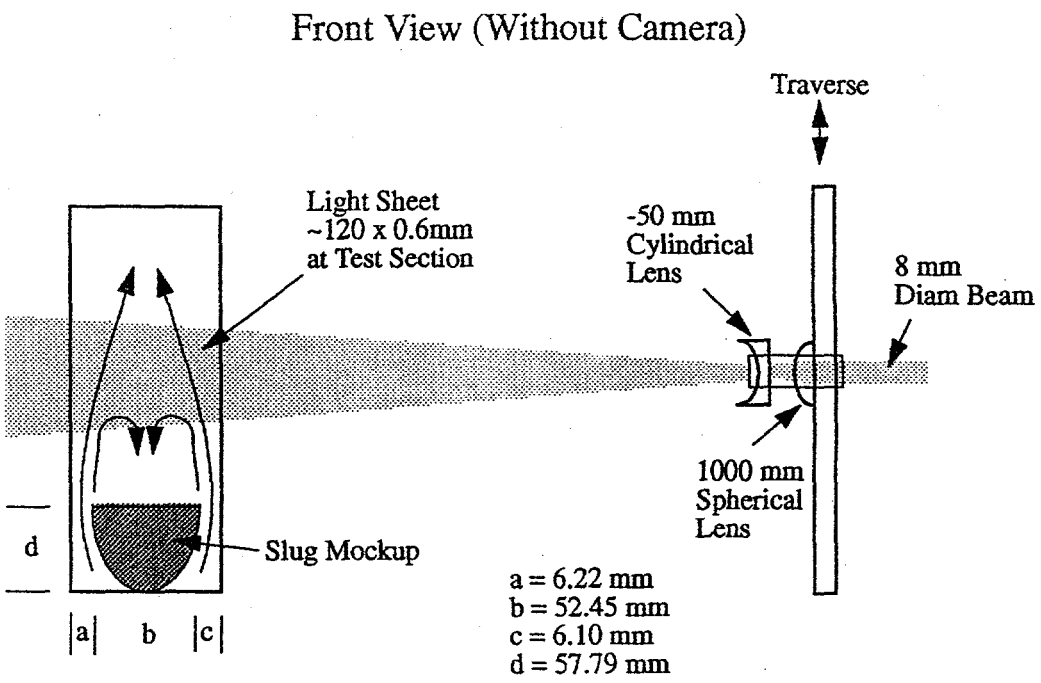

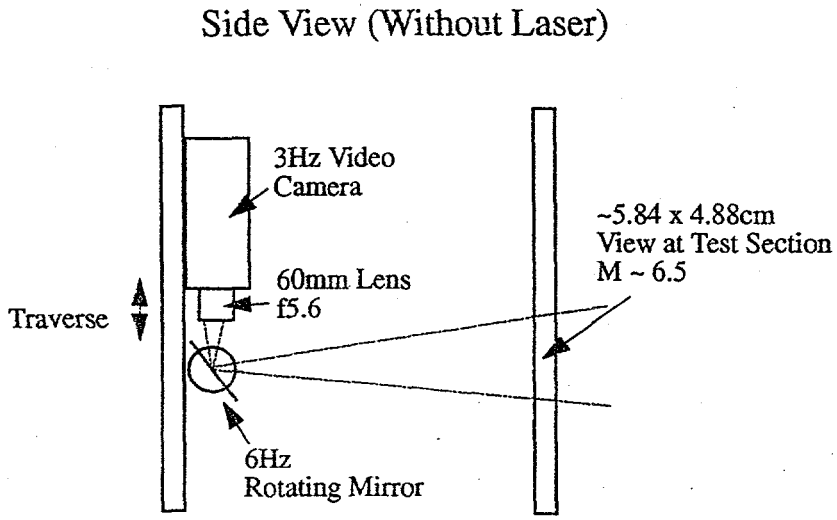

Figure 1. Schematic of experimental set-up. The video camera contained a 1320 x 1100 square pixel array, with a pixel size of 6.8 μm. The magnification factor (M) for the experiments was determined by taking an image of a scale, and measuring the number of pixels over a known distance. The flow rate around the slug obstruction was measured within ±5%.

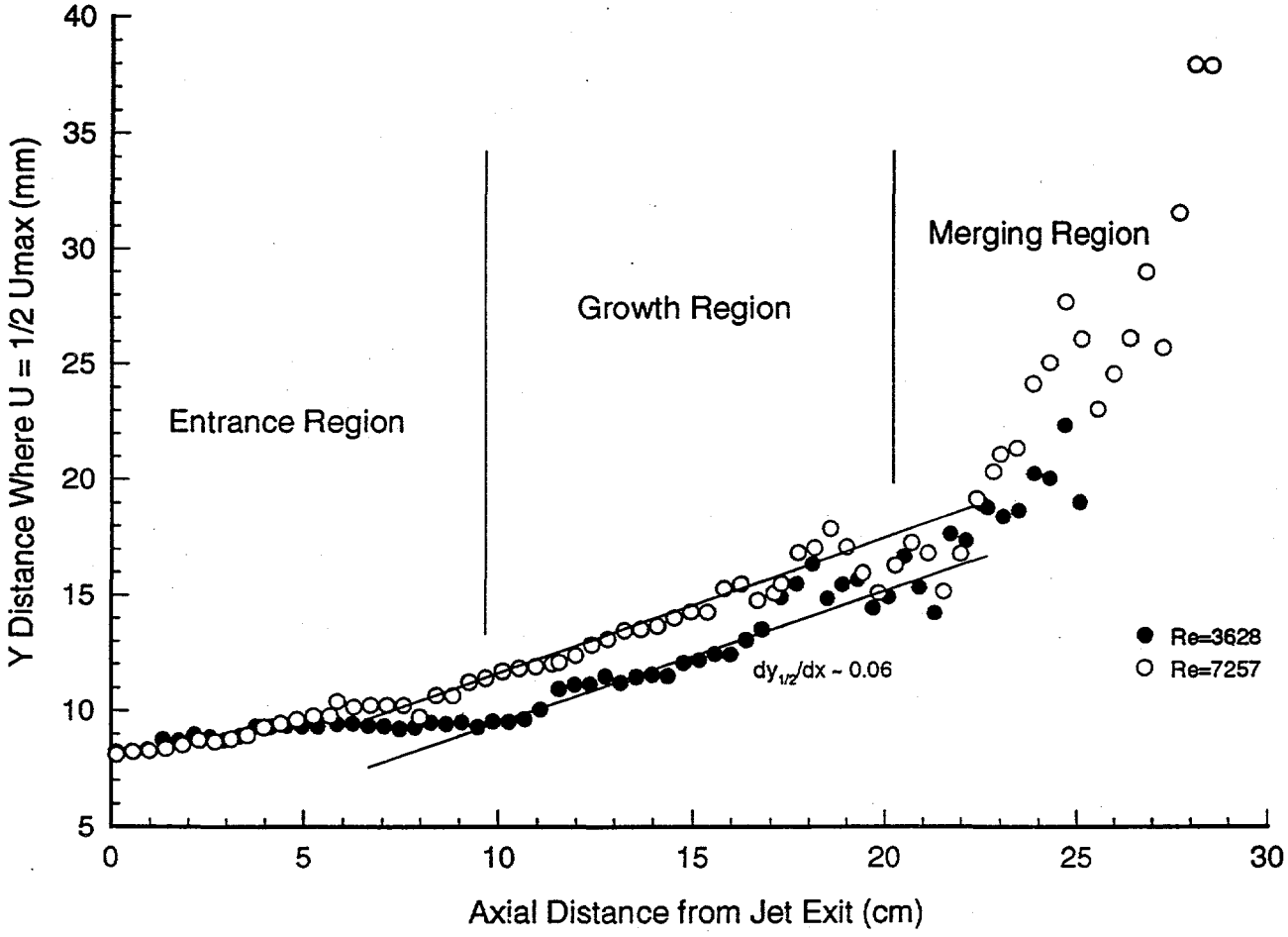

Figure 4. Growth of Half-Width of Wall Jet

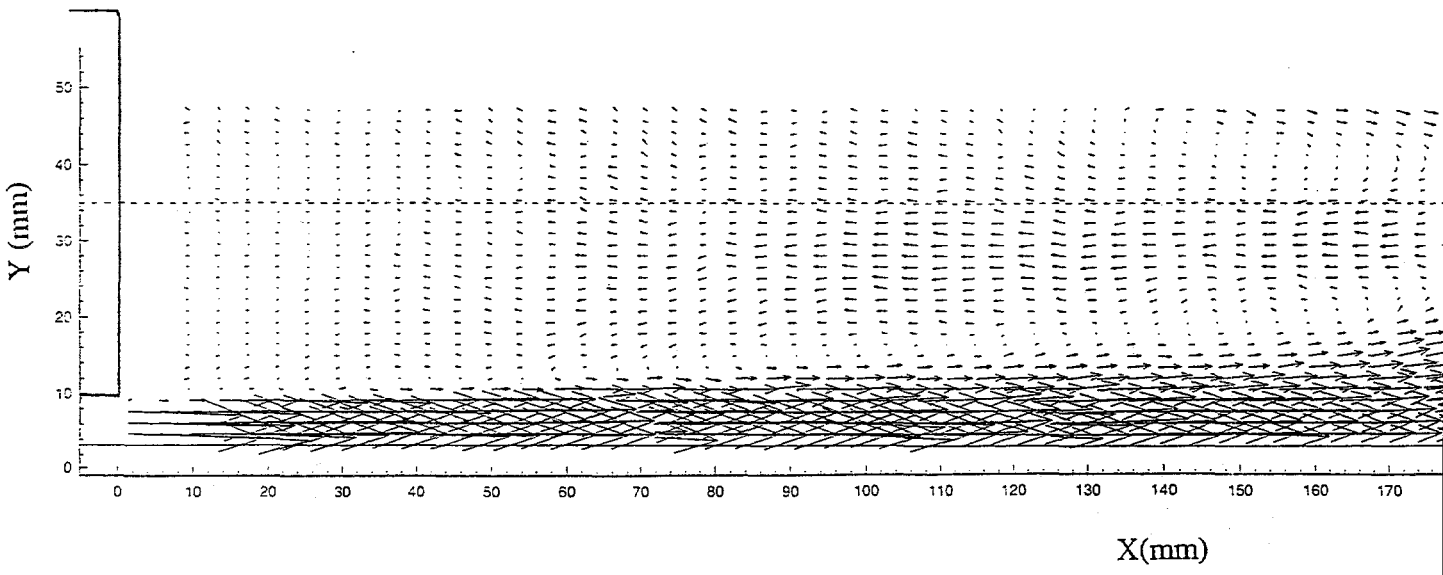

Figure 2. Wake Velocity Field $U_{mean} = 0.16m/s \pm 0.0$

PIV Parameters

laser energy = 100mJ/pulse	magnification = 6.45
light sheet thickness = 0.6mm	spot size = 2.63 x 2.63 mm (
pulse separation = 200μsec	grid spacing = 1.3mm
image shift = 64 pixels	processing algorithm: 1-fra

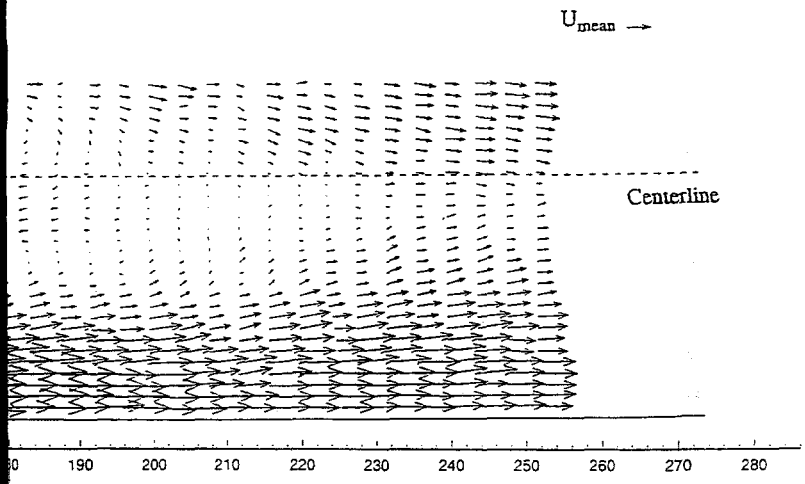

$8m/s$, Re_{jet} = 3628

pixels)

e cross-correlation

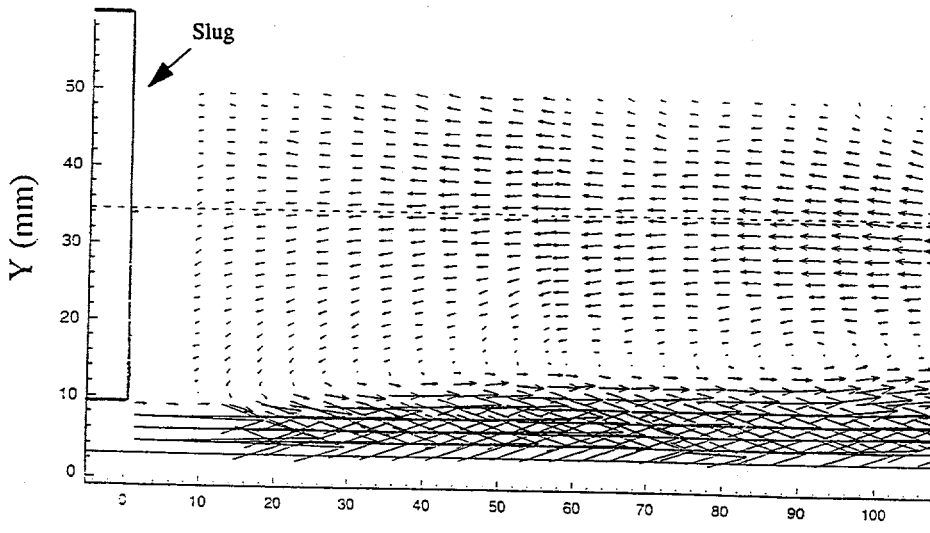

Figure

laser ener
light sheet
pulse sepa
image shif

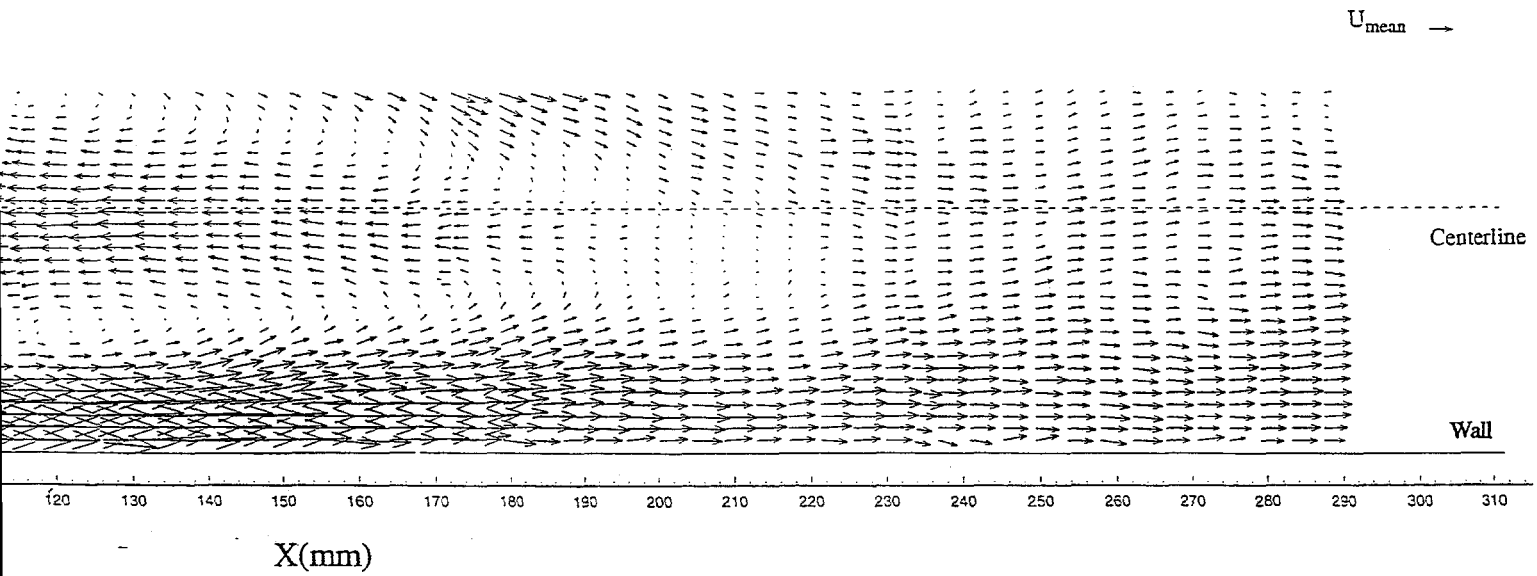

Wake Velocity Field $U_{mean} = 0.32m/s \pm 0.016m/s$, $Re_{jet} = 7257$

PIV Parameters

= 100mJ/pulse	magnification = 6.8
ickness = 0.6mm	spot size = 2.77 x 2.77 mm (60 pixels)
ion = 200μsec	grid spacing = 1.39mm
64 pixels	processing algorithm: 1-frame cross-correlation